

# Plastic deformation of rough metallic surfaces

A. Tiwari,<sup>1,2</sup> A. Almqvist,<sup>3</sup> and B. N. J. Persson<sup>1,2</sup>

<sup>1</sup>*PGI-1, FZ Jülich, Germany*

<sup>2</sup>*www.MultiscaleConsulting.com*

<sup>3</sup>*Machine Elements, Luleå University of Technology, Luleå 97187, Sweden*

We present experimental and theoretical results for the surface topography of a plastically deformed metallic (aluminum) block. When a hard spherical body (here a steel-, silica glass- or silicon nitride ball) with a smooth surface is indented in a metal block with a nominally flat, but still rough, surface, a spherical-cup-like indentation result due to plastic flow. The surface roughness in the indented region is, however, not entirely flattened. The long wavelength (macroasperity) content of the roughness result from the roughness on the original (aluminum) surface, but now plastically deformed. The roughness at short length scale, in the plastically deformed macroasperity contact regions, result from the roughness on the hard ball, and from inhomogeneous plastic flow.

We model the contact mechanics using the boundary element method, combined with a simple numerical procedure to take into account the plastic flow. The theory can semi-quantitatively describe the modification of the roughness by the plastic flow. Since the fluid leakage of metallic seals in most cases is determined by the long wavelength roughness, we predict that the leakage can be estimated based on the elastoplastic contact mechanics model employed here.

The plastic deformations of surfaces of some glassy polymers is very different from what we observed for aluminum, which we attribute to strong work-hardening and to inhomogeneous plastic flow for the polymers. Thus the numerical procedure to account for the plastic flow proposed here cannot be applied to glassy polymers in general.

## 1 Introduction

The contact between metallic bodies occur in many applications, and often the contact pressure is so high as to generate plastic deformation, at least at the asperity level[1–10]. In fact, because of surface roughness and the high elastic modulus of most metals, the contact pressure between asperities at short length scale can be very high even when the nominal contact pressure is low. Thus for metals in the area of real contact some plastic flow will almost always occur, at least during the first contact[11].

Metallic seals are used in many applications involving very high fluid pressure differences, and in ultra high vacuum systems. Surface roughness and plastic flow highly affects leakage in metallic seals, since they are key factors in determining the surface separation in the non-contact area. For elastic solids like rubber, contact mechanics theories have been developed for how to predict the fluid leakage rate, and it has been shown that they are in good agreement with experiments[12, 13]. The simplest approach assumes that the whole fluid pressure difference between the inside and outside of the sealed region, occur over the most narrow constrictions (denoted critical junctions), encountered along the largest open percolating non-contact flow channels.

For elastic solids numerical contact mechanics models[14], such as the boundary element model, and the analytic theory of Persson[15, 16], can be used to calculate the surface separation at the critical junction and hence predict fluid leakage rates. For solids involving plastic flow, the surfaces will approach each other more closely than if only elastic deformations would occur. This will reduce the fluid leakage rate[17, 18].

Here we will present the outcome of a study, where we

experimentally explore the nature of the plastic deformation of the asperities of a sandblasted aluminum surface, but we believe the results should hold quite generally for other metals of interest such as steel, copper or bronze. We will also present results from numerical simulations of the experimental set-up, based on the boundary element method combined with a simple procedure to include plastic flow. More precisely, we employ the method presented in[19] that assumes an elastoplastic model where a solid deforms elastically until the local pressure reaches a critical stress (the penetration hardness), after which it flows without strain hardening.

Recently, several studies of surface roughness and plastic flow have been reported using microscopic (atomic) models[20], or models inspired by atomic scale phenomena that control the nucleation and glide of the dislocations[21–23]. These models supply fundamental insight into the complex process of plastic flow, but are not easy to apply to practical systems involving inhomogeneous polycrystalline metals and alloys exhibiting surface roughness of many length scales. The approach we use here is less accurate but easy to implement, and it can be used to estimate the leakage rates of metallic seals. It remains, however, to test in detail how accurate the results are.

## 2 Experimental

The aluminum block was indented with either a steel ball with 50 mm diameter, or a silicon nitride  $\text{Si}_3\text{N}_4$  ball with 33.338 mm diameter, or a borosilica glass ball with the diameter 30 mm. The normal (indentation) force was 40 kN. Indentation was done on a rectangular aluminum block with a polished surface, and on two sandblasted

aluminum surfaces. The sandblasting was done with glass beads (spherical particles with smooth surfaces) of diameter  $\approx 10 \mu\text{m}$  for a time ranging from 5 to 8 minutes using 8 bar air pressure. The topography measurements were performed with Mitutoyo Portable Surface Roughness Measurement device, Surftest SJ-410 with a diamond tip with the radius of curvature  $R = 1 \mu\text{m}$ , and with the tip-substrate repulsive force  $F_N = 0.75 \text{ mN}$ . The lateral tip speed was  $v = 50 \mu\text{m/s}$ .

From the the measured surface topography (line scans)  $z = h(x)$  we calculated the one-dimensional (1D) surface roughness power spectra defined by

$$C_{1D}(q) = \frac{1}{2\pi} \int dx \langle h(x)h(0) \rangle e^{iqx} \quad (1)$$

where  $\langle \dots \rangle$  stands for ensemble averaging. For surfaces with isotropic roughness the 2D power spectrum  $C(q)$  can be obtained directly from  $C_{1D}(q)$  as described elsewhere[24, 25]. For randomly rough surfaces, all the (ensemble averaged) information about the surface is contained in the power spectrum  $C(q)$ . For this reason the only information about the surface roughness which enter in contact mechanics theories (with or without adhesion) is the function  $C(q)$ . Thus, the (ensemble averaged) area of real contact, the interfacial stress distribution and the distribution of interfacial separations, are all determined by  $C(q)$ [15, 16]. Note that, the moments of the power spectrum determines the often quoted standard quantities, which are output of most stylus instruments. Thus, for example, the mean-square (ms) roughness amplitude  $\langle h^2 \rangle$  and the ms slope  $\langle (dh/dx)^2 \rangle$  are given by

$$\langle h^2 \rangle = 2 \int_0^\infty dq C_{1D}(q),$$

and

$$\langle (dh/dx)^2 \rangle = 2 \int_0^\infty dq q^2 C_{1D}(q),$$

respectively.

Since the surface topography was measured only along line scans  $z = h(x)$ , for the numerical contact mechanics simulations (see Sec. 4) we produced randomly rough surfaces using the random-phase-method described in Appendix D in Ref. [26]. For generating these surfaces we used the 2D surface roughness power spectra obtained as described above.

### 3 Experimental results

We have performed indentation experiments for three different nominally flat aluminum surfaces, one polished and two sandblasted. Before performing the indentation experiments we measured the surface topography  $z = h(x)$  along several 10 mm long tracks, from which we have calculated the 1D surface roughness power spectra using (1).

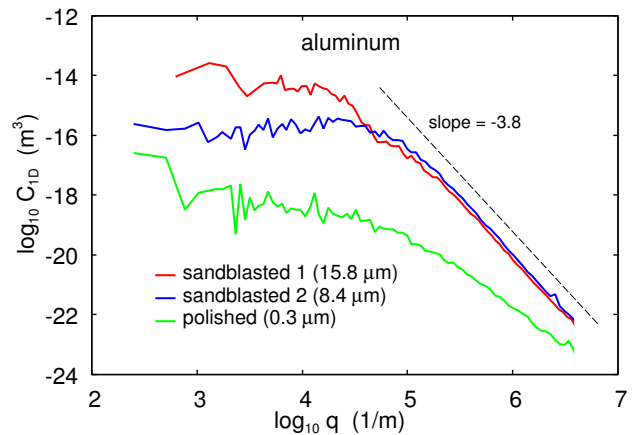


FIG. 1: The surface roughness power spectrum as a function of the wavenumber (log-log scale) for two sandblasted aluminum surfaces and one polished aluminum surface. The root-mean-square (rms) roughness amplitude of the three surfaces are  $h_{\text{rms}} = 15.8, 5.8$  and  $0.3 \mu\text{m}$ . The corresponding rms slopes are 0.42, 0.45 and 0.04, respectively. The surfaces have nearly vanishing skewness and the kurtosis is close to 3 for all the surfaces.

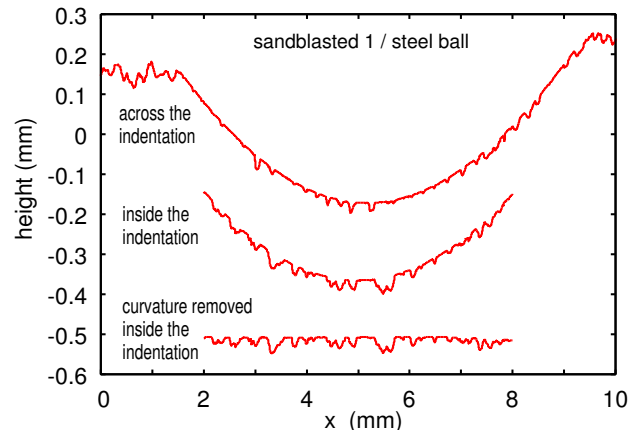


FIG. 2: The surface roughness height profile  $h(x)$  of the sandblasted aluminum surface 1 after squeezing a steel ball (radius  $R = 2 \text{ cm}$ ) against the aluminum block with the axial force  $F_N = 40 \text{ kN}$  for 1 minute. This result in a spherical cup indentation with the same radius of curvature as the steel ball and with the indentation diameter  $\approx 0.8 \text{ cm}$ . The middle line shows the line scan data from inside the indentation, and the bottom line after removing the macroscopic curvature. Note that the high asperities have flat upper surfaces because of plastic flow.

Figure 1 shows the surface roughness power spectra as a function of the wavenumber (log-log scale) for the sandblasted and polished aluminum surfaces. The root-mean-square (rms) roughness amplitude of the three surfaces are  $h_{\text{rms}} = 15.8, 5.8$  and  $0.3 \mu\text{m}$ , and the corresponding rms slopes are 0.42, 0.45 and 0.04, respectively. The surfaces have nearly vanishing skewness ( $-0.02, 0.13$  and  $-0.05$ ), and the kurtosis (2.7, 2.9 and 3.1) is close to 3 for

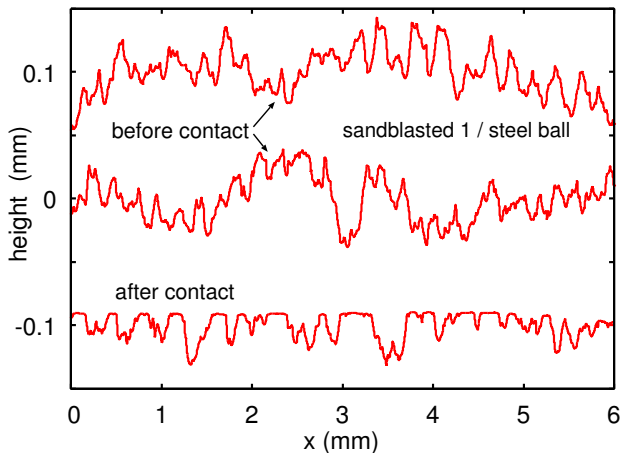


FIG. 3: The surface roughness height profile  $h(x)$  of the sandblasted aluminum surface 1 (top two lines), and after squeezing the steel ball against the aluminium surface (bottom line). The bottom linescan data is from inside the indentation by first removing the macroscopic curvature. Note that the high asperities have flat upper surfaces because of plastic flow.

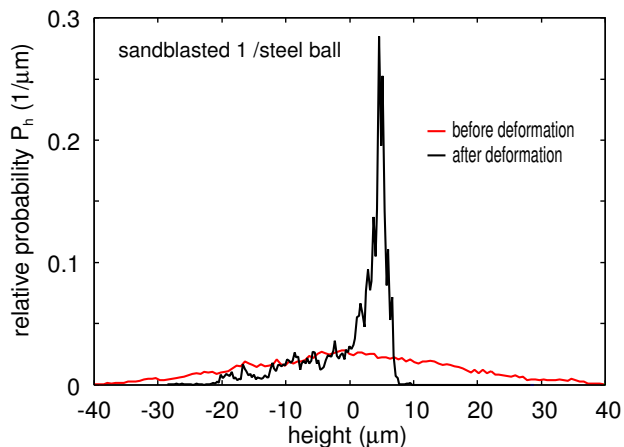


FIG. 4: The surface roughness height distribution  $P_h$  of the sandblasted aluminum surface 1 (red line), and after squeezing the steel ball against the aluminum block (black line). The black line is obtained from the line scan data inside the indentation by first removing the macroscopic curvature. The sharp peak is due to the high asperities have flat upper surfaces (of equal height) because of plastic flow.

all the surfaces, as expected for randomly rough surfaces with a Gaussian height probability distribution.

The sandblasted surface 1 was squeezed against a smooth steel ball, and the sandblasted surface 2 and the polished surface was squeezed against the ceramic ball and the silica glass ball, in all cases with the normal force 40 kN for 1 minute.

Figure 2 shows the surface roughness height profile  $h(x)$  of the sandblasted aluminum surface 1 after squeezing it against the steel ball. The spherical cup indenta-

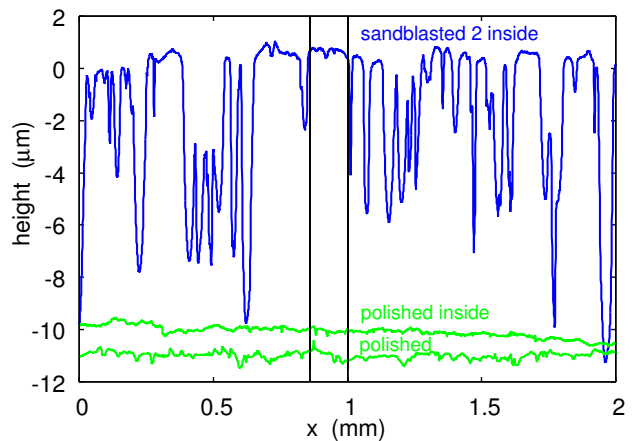


FIG. 5: The surface topography of the sandblasted aluminum surface 2 (top blue line), and of the polished surface, indented with a ceramic ball (Silicon nitride,  $\text{Si}_3\text{N}_4$ ) with diameter 33.3 mm. The axial force  $F_N = 40$  kN for 1 minute. The topography (middle line) is after removing the surface curvature. Also shown is the surface topography of the not indented surface area of the polished ball (bottom green line).

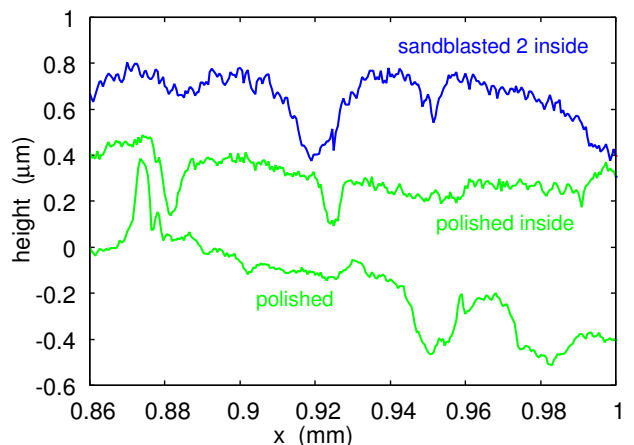


FIG. 6: The surface topography in Fig.5 between the two vertical lines.

tion has nearly the same radius of curvature as the steel ball, and with the indentation diameter  $\approx 0.8$  cm. Also shown in the figure is a line scan from inside the indentation, before and after removing the macroscopic curvature. Note that the high asperities have flat upper surfaces because of plastic flow, while the roughness in the big valleys are left almost unchanged. This is very different from what we observed in Ref. [27] for glassy polymers, where during plastic deformation material moved effectively from the top of asperities to the nearby valley, resulting in long wavelength roughness which appeared the same as on the original (undeformed) surface but with smaller amplitude. We attributed this to strong work-hardening. The aluminum surface is most likely already work-hardened by the production procedure, and

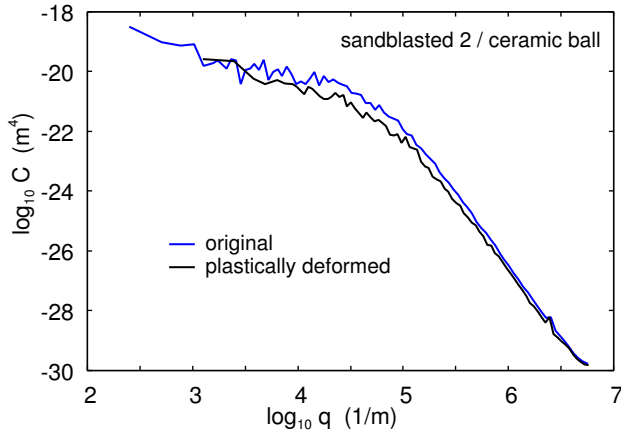


FIG. 7: The surface roughness power spectrum as a function of the wavenumber (log-log scale) before indentation (blue), and after (black) plastic deformation. For the sandblasted surface 2 indented by the ceramic ball.

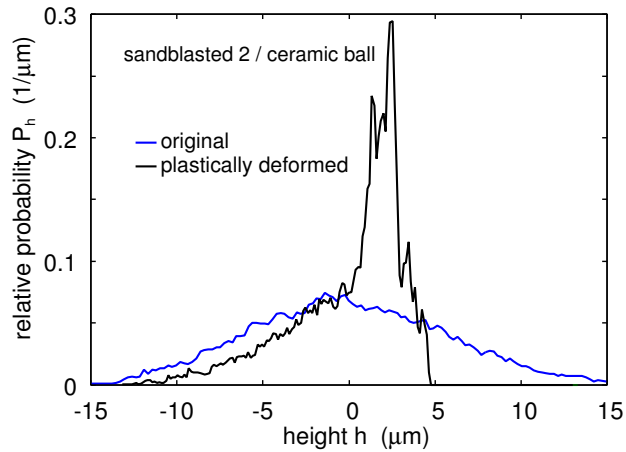


FIG. 8: The height probability distribution of the sandblasted surface 2 (blue line), and after indenting it with the ceramic ball (black line). The height probability distribution of the indented surface is from inside the indented region after removing the surface curvature.

this could explain the very different nature of the plastic flow in the two cases.

Usually the material penetration hardness is defined as the ratio between the external normal force (here  $F_N = 40$  kN) and the projected indentation area (here  $A_0 = \pi r_0^2$  with  $r_0 \approx 4$  mm). This gives  $\sigma_P \approx 0.8$  GPa. However, note that only  $\approx 50\%$  of the nominal contact area in Fig. 2 appears to be plastically deformed. In fact, if a plastically deformed macroasperity contact area is observed at higher magnification, then short wavelength roughness can be observed, and an even smaller fraction than  $\approx 50\%$  of the nominally contact area is plastically deformed (see also discussion below). We conclude that most likely the penetration hardness depends on the length scale (or size of the indenter), a fact which is

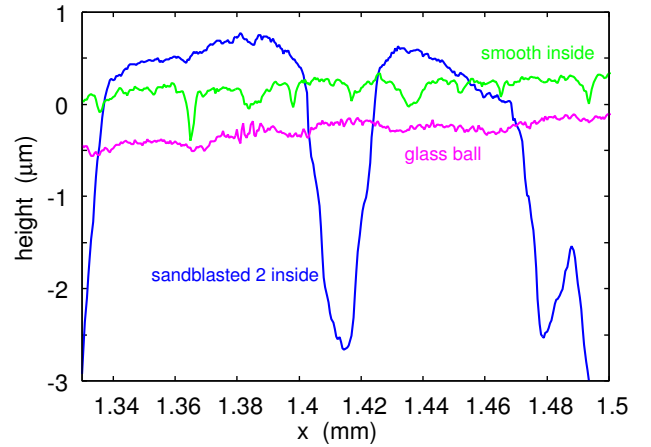


FIG. 9: The surface roughness height profile  $h(x)$  of the sandblasted aluminum surface 2 after squeezing a glass ball (radius  $R = 1.5$  cm) against the aluminum block with the axial force  $F_N = 40$  kN for 1 minute (blue line). This result in a spherical cup indentation with nearly the same radius of curvature as the glass ball. The green line is the same result for a polished aluminum surface. The pink line is the topography of the glass ball. In all cases the curvature of the indentation (or the glass ball) is removed.

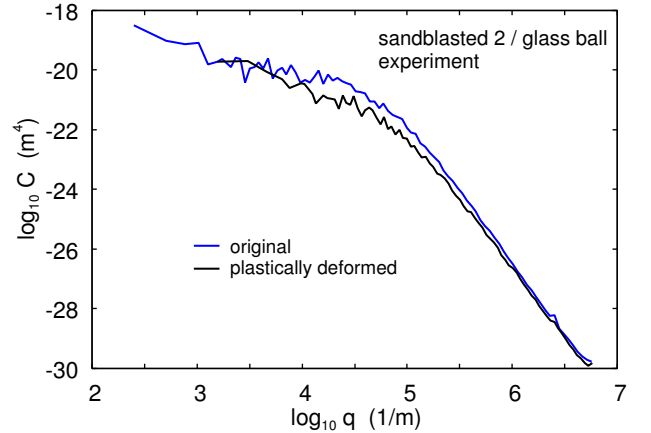


FIG. 10: The surface roughness power spectrum as a function of the wavenumber (log-log scale) before indentation (blue), and after (black) plastic deformation. For the sandblasted surface 2 indented by the glass ball and after removing the curvature of the indentation.

well known from earlier studies using different size of the indenter, or different indentation depth[28]. There are several different reason for this length-scale dependent hardness, e.g., it may result from a thin work-hardened surface layer.

Figure 3 shows magnified pictures of the surface topography in Fig. 2. The two upper curves are linescans from the sandblasted surface 1 before plastic deformation, and the lower curve shows a linescan from inside the indented region by first removing the macroscopic curvature. Note that the high asperities (at this magnification) appear to

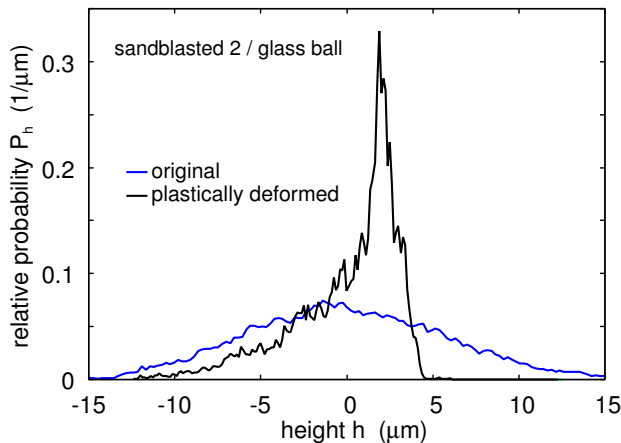


FIG. 11: The height probability distribution of the sandblasted surface 2 (blue line), and after indenting it with the glass ball (black curve). The height probability distribution of the indented surface is from inside the indented region after removing the surface curvature.

have flat upper surfaces because of plastic flow.

Figure 4 shows the surface roughness height distribution  $P_h$  of a sandblasted aluminum surface 1 before (red line), and after (black line) squeezing the steel ball against the aluminum block. In the latter case the line scan data is from inside the indentation and obtained by first removing the macroscopic curvature. The sharp peak is due to the flat upper surfaces of the plastically deformed asperities.

The blue line in Fig. 5 shows the surface topography of the sandblasted surface 2 after indenting it with the ceramic ball. The linescan is from inside the indented region after removing the surface curvature. Similar result for the polished aluminum surface is shown by the upper green line. The lower green line is the measured surface topography of the polished aluminum surface before indenting it with the ball.

Figure 6 shows a magnified view of segments from the roughness profiles in Fig. 5 (the region between the two vertical lines). Note that the short-wavelength roughness in the plastically deformed region of the sandblasted surface (blue line), is very similar to that in the indented region of the polished surface (upper green line), and slightly larger than that of the original polished surface (green line). The short wavelength roughness is mainly due to the surface roughness of the ceramic ball (not shown), but in addition some contribution to the roughness may be due to inhomogeneous plastic flow.

Figure 8 shows the height probability distribution for the sandblasted surface 2 (original surface) (blue), and of from inside the indented region after removing the surface curvature (black).

We have also performed indentation studies using a glass ball. The blue line in Fig. 9 shows the surface roughness height profile  $h(x)$  of the sandblasted aluminum sur-

face 2 after squeezing the silica glass ball against the aluminum block. The green line is the same result for the polished aluminum surface and the pink line is the topography of the glass ball. Note that the short wavelength roughness of both the sandblasted and polished aluminum surface are very similar to that of the glass ball. This is due to the plastic imprint of the glass ball roughness in the contact regions with the aluminum surface. Recall that the penetration hardness of the silica glass is several times higher than that of the aluminum so only the aluminum will flow plastically.

Figure 10 shows the surface roughness power spectrum as a function of the wavenumber (log-log scale) before indentation (blue), and after (black) plastic deformation. The results are for the sandblasted surface 2 indented by the glass ball.

Figure 11 shows the height probability distribution of the sandblasted surface 2 (blue line), and after indenting it with the glass ball (black curve). The height probability distribution of the indented surface is from inside the indented region after removing the surface curvature.

#### 4 Numerical simulation

We have performed numerical simulations of the plastic deformation of rough surfaces. We use the boundary element method (BEM) first described in [19], which treats the elastic deformations exactly (within the small slope approximation), and the plastic deformations is considered within the elastoplastic approximation. In this model the solid deform elastically as long as the surface stress is below the penetration hardness  $\sigma_P$ . When the local stress reach the penetration hardness, the solid flow plastically without work hardening. In the model the plastic flow is taken into account by moving the surface grid point downwards in such a way that the local stress in the plastically deformed area is always equal to the penetration hardness. The numerical solution procedure is based on spectral theory, and an FFT-accelerated approach is applied to increase the computational efficiency. Inputs to the model is the geometries and roughness of the contacting bodies, their Young's modulus of elasticity, the Poisson ratios, and the indentation hardness of the softer of the two surfaces. It predicts the contact pressure distribution and the corresponding elastic and plastic deformations of the contacting bodies. Parameters like the real area of contact, the ratio of plastically deformed to the nominal contact area, can also be deduced by postprocessing the results. This BEM-based elastoplastic approach has also been frequently employed in other works, see e.g. [16, 18, 29–34].

We have performed calculations for the sandblasted surface 2. Since the topography of this surface was measured only along a line, we first calculated the 2D surface roughness power spectrum from the 1D power spectrum [24, 25]. Next we generated mathematically a randomly rough surface with the powers spectrum of sur-

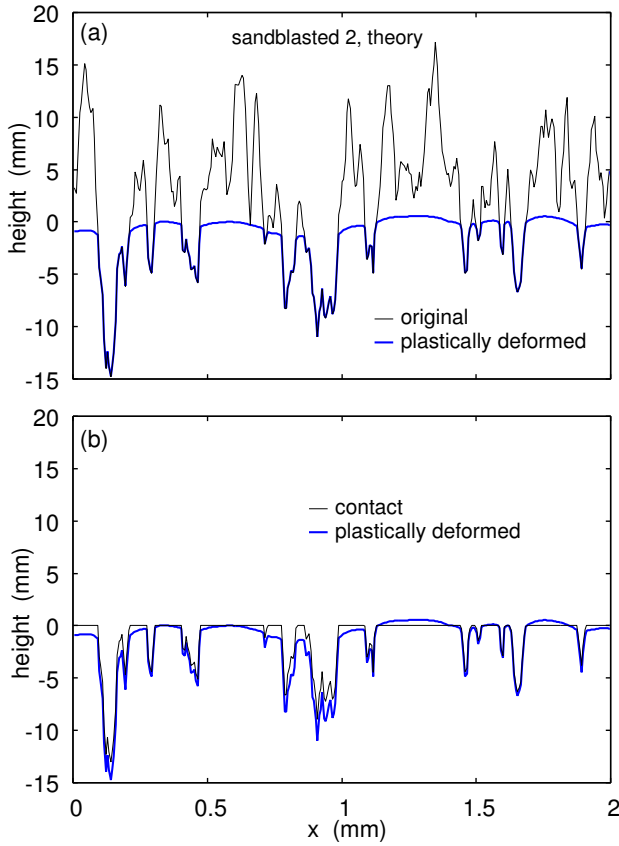


FIG. 12: Calculated plastic and elastoplastic deformations due to a load corresponding to the nominal contact pressure 1 GPa. Depicted in (a) are the original surface topography (thin line), and the plastically deformed profile (thick line), and depicted in (b) are the surface topography during contact with a flat surface (thin line), and the plastically deformed profile (thick line).

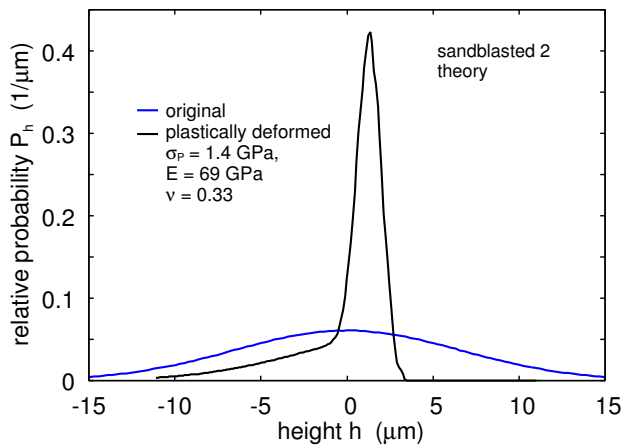


FIG. 13: The calculated height probability distribution before (blue) and after (black) squeezing the rough surface against a perfectly smooth surface with the nominal contact pressure 1 GPa.

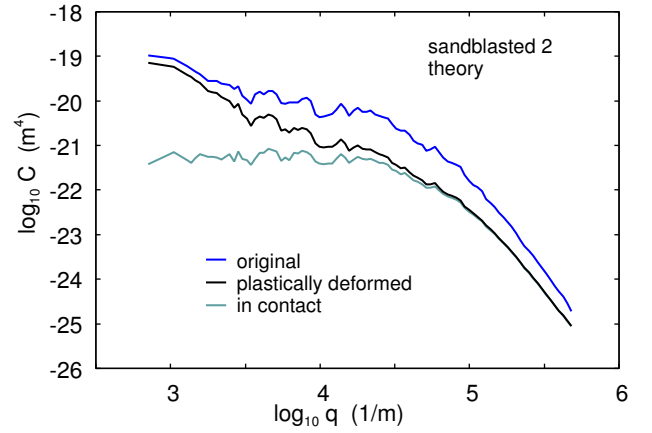


FIG. 14: The calculated surface roughness power spectrum as a function of the wavenumber (log-log scale) before indentation (blue), and after (black) plastic deformation with the nominal contact pressure 1 GPa, and of the deformed surface during indentation (contact pressure 1 GPa) (gray).

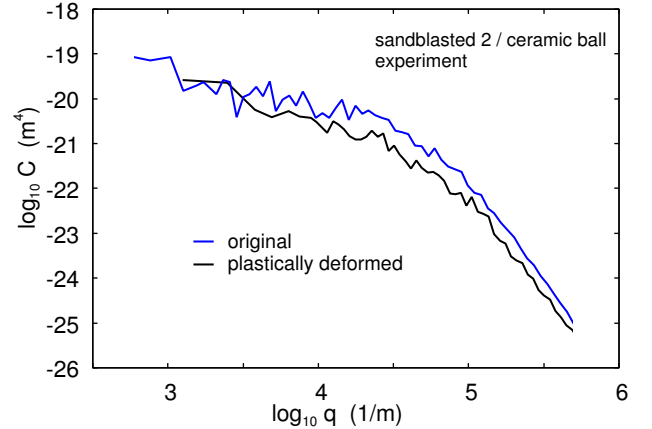


FIG. 15: The measured surface roughness power spectrum (for the ceramic ball on the sandblasted surface 2) as a function of the wavenumber (log-log scale) before indentation (blue), and after (black) plastic deformation. The same as in Fig. 7 but plotted on a reduced wavenumber scale.

face 2 using the procedure described in Appendix D in Ref. [26]. However, we have not used the full power spectrum as this would result in a surface with roughness over too many length scales or degrees of freedom. Thus, the surface we use has the size  $2048 \times 2048$  grid points, and reproduce the measured power spectrum for  $q < q_1$  with  $q_1 \approx 5 \times 10^5 \text{ m}^{-1}$ .

We consider now squeezing a rigid and perfectly flat surface against an elastoplastic solid with the surface roughness obtained as described above. We assume the nominal contact pressure 1 GPa which is similar as the nominal contact pressure acting in the indented region in the experiments. We assume the Young's elastic modulus  $E = 69 \text{ GPa}$ , the Poisson ratio  $\nu = 0.33$ , which are typical values for aluminum. We also assume the aluminum

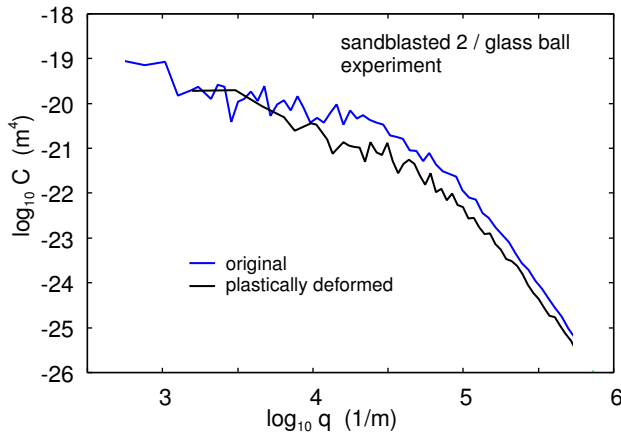


FIG. 16: The measured surface roughness power spectrum (for the glass ball on the sandblasted surface 2) as a function of the wavenumber (log-log scale) before indentation (blue), and after (black) plastic deformation. The same as in Fig. 10 but plotted on a reduced wavenumber scale.

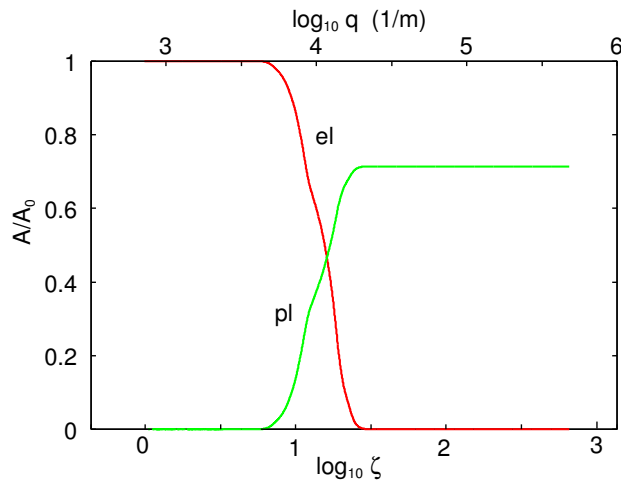


FIG. 17: The relative contact area  $A/A_0$  as a function of the magnification  $\zeta$  (lower log-scale) or as a function of the wavenumber  $q = \zeta q_0$  (upper log-scale) as obtained using the Persson contact mechanics theory with the power spectrum shown in Fig. 14 (blue line). The relative elastic contact area and plastic contact area are shown separately as the red and green lines, respectively. In the calculation we have used the elastoplastic parameters given in the text.

penetration hardness 1.4 GPa.

The rough surface has the size  $L \times L$  with  $L \approx 12.5$  mm. In Fig. 12 we show a 2 mm long line scan of the the calculated surface topography. In (a) we show the original surface topography (thin line), and of the plastically deformed profile (thick line). In (b) we show the surface topography during contact with a flat surface (thin line), and of the plastically deformed profile (thick line). Note that in (b) the elastic rebound makes the upper surface of the plastically deformed asperities curved. Note also in (a) that the surface roughness below the plastically

deformed region is unchanged. Since the total volume of the solid must be (nearly) unchanged, in reality material must flow also in the tangential direction, which result in some modification of the roughness also in the regions which was not in contact with the flat countersurface. For materials which undergoes work hardening this tangential flow becomes very important and can result in a complete breakdown of the plastic flow procedure used in the present paper, as indeed observed for polyethylene in Ref. [27] (see also Discussion).

Figure 13 shows the calculated height probability distribution before (blue) and after (black) squeezing (and removing) the rough surface against the flat rigid countersurface. Both the original and plastically deformed surface have similar height distribution as observed in the experiment (compare to Fig. 8 and Fig. 11).

Figure 14 shows the calculated surface roughness power spectrum as a function of the wavenumber (log-log scale) before indentation (blue), and after plastic deformation (black). Also shown is the power spectrum of the surface of the solid when in contact with the flat rigid countersurface (gray). Note that for large wavenumber the plastically deformed surface and the surface in contact with the flat rigid surface exhibit the same surface roughness power spectrum. This is due to the fact that the large wavenumber roughness is due to the surface roughness in the regions not in contact with the flat surface, and this part is nearly unchanged. However, the surface area occupied by this (nearly unchanged) surface roughness is smaller than for the original surface, and this explain why the power spectrum for large wavenumbers of the plastically deformed surface is smaller than for the original surface.

In order to compare the measured power spectrum with the calculated ones, we show again in Fig. 15 and Fig. 16 the measured power spectra (from Fig. 7 and Fig. 10) but now on the same wavenumber interval as in Fig. 14. Comparing Fig. 14 with Fig. 15 and 16, we conclude that the calculated power spectrum of the plastically deformed surface is similar to the measured one, but shows a slightly larger reduction in the magnitude of  $C(q)$  then the measured one. This may indicate that the penetration hardness we used is slightly too small, but we have made no attempt to optimize the agreement with the experiments by changing the magnitude of  $\sigma_P$ .

The Persson contact mechanics theory[15] can be used to study the nature of the contact area as we increase the magnification. When we study the interface at the magnification  $\zeta$  we only observe surface roughness with wavenumber  $q < \zeta q_0$ , where  $q_0$  is the smallest wavenumber. Thus for  $\zeta = 1$  (or  $\log_{10}\zeta = 0$ ) we do not observe any roughness and since the nominal contact pressure  $p = 1$  GPa is below the penetration hardness  $\sigma_P = 1.4$  GPa there is no plastic deformation, i.e.  $A_{el}/A_0 = 1$  and  $A_{pl}/A_0 = 0$ . When we increase the magnification we observe surface roughness and the contact area decreases

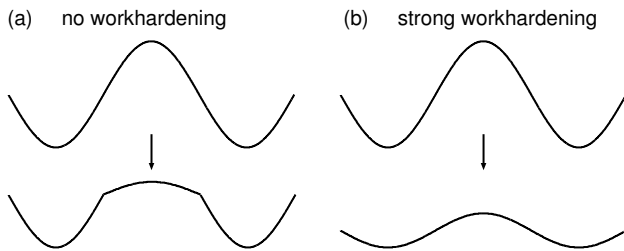


FIG. 18: Two limiting behavior of the plastic deformation of a surface sinus-roughness-component. (a) For a material without work hardening (e.g., a material already strongly work hardened) the plastic flow is localized to the region where the solid make contact with the countersurface, here assumed to be a flat rigid surface. (b) For a material which undergoes strong work hardening the flow of material is more long range, resulting in material transfer to the valley region, effectively resulting in a sinus profile with smaller amplitude.

and the contact stress increases until it becomes large enough to induce plastic flow.

Figure 17 shows the relative contact area  $A/A_0$  as a function of the magnification  $\zeta$  (lower scale) or as a function of the wavenumber  $q = \zeta q_0$  (upper scale) as obtained using the Persson contact mechanics theory with the power spectrum shown in Fig. 14 (blue line). The relative elastic contact area and plastic contact area are shown separately as the red and green lines, respectively. In the calculation we have used the same elastoplastic parameters as in the numerical simulations using the BEM-based approach.

The result in Fig. 17 are consistent with the power spectra shown in Fig. 14-16. Thus, Fig. 17 shows that the long wavelength roughness components for  $\log_{10} q < 3.5$  are elastically deformed, and this explain why in this wavenumber region the power spectrum of the plastically deformed surface is close to that of the original surface in Fig. 14-16. For  $\log_{10} q > 4.2$  the Persson theory predict that the contact is fully plastic which explain why the power spectrum of the plastically deformed surface is the same in and out of contact with the flat surface in this wavenumber region.

## 5 Discussion

The simple procedure used above to describe the plastic flow produces plastically deformed surfaces with height probability distributions and surface roughness power spectra in semi-quantitative agreement with the experimental data. In our study we used an aluminum block, but the results are probably applicable for other metals as well, assuming negligible work hardening so the simple elastoplastic description with a constant penetration hardness is a reasonable approximation. However, the following points need to be taken into consideration:

(a) The penetration hardness depends on the length scale. Suppose we indent a solid with a rigid perfectly smooth sphere. If we look at the indentation at low mag-

nification we do not see any surface roughness and we would calculate the penetration hardness  $\sigma_P = F_N/A_0$ , where  $A_0 = \pi r_0^2$  is the projected contact area (a circular area). This is, in fact, the standard definition of the penetration hardness. However, in general we do not make plastic contact everywhere within the apparent (projected) contact area  $A_0$ . It is clear from this fact that the penetration hardness at the asperity length scale must be higher than at the macroscopic length scale. If we increase the magnification further we may observe that within the plastically deformed (macro) asperity contact regions there may be regions which are not plastically deformed, corresponding to an even higher penetration hardness at even shorter length scale. To obtain the correct contact mechanics observed at high magnification is necessary to include the length (or magnification) dependency of the penetration hardness.

(b) At very short length scale the plastic flow may be inhomogeneous. This implies that if one indent a perfectly smooth surface of a solid with a spherical ball with perfectly smooth surface, roughness may be generated in the indented surface area[20]

(c) The procedure used above to describe the plastic flow gives plastically deformed surfaces with roughness in relative good agreement with experiment for the aluminum block we used. But this result is expected only if there is no work hardening. The aluminum block we used has probably already undergone strong work hardening during the preparation process, and the results presented above may not be valid for a thermally annealed metal block. In an earlier study we have found that for some polymers, in particular polyethylene, the plastically deformed surface exhibit a perfectly symmetric Gaussian-like height probability distribution, in contrast to the strongly skewed height distribution we observe for aluminum (see Fig. 8 and Fig. 13). We interpret this as resulting from strong work hardening, which effectively result in flow of materials, from the top of asperities to the nearby wells as indicated in Fig. 18. Only by assuming this can the experimental data for polymers be understood.

The study presented in this paper is relevant for the fluid leakage in metallic seals. Metallic seals are usually made from steel, copper or bronze, and these metals usually have work hardened surface layers and should deform plastically in a similar way as the aluminum block studied here. Thus, we believe that the theory approach used here in combination with, e.g. the critical junction theory, may be used to estimate the leakage of metallic seals. Such an (experimental and theory) study will be reported on elsewhere[35].

## 6 Summary and conclusion

We have presented experimental and matching computer simulation results pertaining to indentation of rough aluminum surfaces with balls made of steel, ce-

ramic and silica glass. We found that the BEM-based approach, with a simple way to include plasticity within the elastoplastic model description, can be used to predict the height probability distribution and the surface roughness power spectra of the plastically deformed surfaces. The experimental- and the numerical simulation results, are also consistent with the predictions of the Persson contact mechanics theory for the elastic and plastic contact area as a function of the magnification. The contact area is of direct importance for the leakage of seals as it determines when the contact area percolate and the leakage vanish. This study, combined with findings in [27], indicate that work hardening will strongly affect the nature of the plastically deformed roughness: for material with strong work hardening there is, at present, no simple numerical approach to predict the surface topography of plastically deformed surfaces.

*Acknowledgments:* BNJP acknowledges support by the DFG-grant: PE 807/12-1.

AA acknowledges support from VR (The Swedish Research Council): DNR 2019-04293.

- 
- [1] B.N.J. Persson, *Sliding Friction: Physical Principles and Applications*, Springer, Heidelberg (2000).
- [2] E. Gnecco and E. Meyer, *Elements of Friction Theory and Nanotribology*, Cambridge University Press (2015).
- [3] J.N. Israelachvili, *Intermolecular and Surface Forces*, (Academic, London), 3rd Ed. (2011).
- [4] J.R. Barber, *Contact Mechanics (Solid Mechanics and Its Applications)*, Springer (2018).
- [5] B.N.J. Persson, *Contact mechanics for randomly rough surfaces*, Surface Science Reports **61**, 201 (2006).
- [6] AI Vakis, VA Yastrebov, J Scheibert, C Minfray, L Nicola, D Dini, A Almqvist, M Paggi, S Lee, G Limbert, JF Molinari, G Anciaux, R Aghababaei, S Echeverri Restrepo, A Papangelo, A Cammarata, P Nicolini, C Putignano, G Carbone, M Ciavarella, S Stupkiewicz, J Lengiewicz, G Costagliola, F Bosia, R Guarino, NM Pugno, MH Müser, *Modeling and simulation in tribology across scales: An overview*, Tribology International (TRIBINT-D-17-01694 - Accepted Manuscript).
- [7] F. Bowden and D. Tabor, *The Friction and Lubrication of Solids*, Number v. 1 in Oxford Classic Texts in the Ph, Clarendon Press (2001).
- [8] J.A. Greenwood, *Contact of rough surfaces*, in Fundamentals of Friction: Macroscopic and Microscopic Processes, 37-56. Kluwer (1992).
- [9] L. Kogut and I. Etsion, *Elastic-Plastic Contact Analysis of a Sphere and a Rigid Flat*, ASME J. Appl. Mech. **69**, 657 (2002)
- [10] H. Ghaednia, X. Wang, S. Saha, Y. Xu, A. Sharma, and R.L. Jackson, *A Review of Elastic-Plastic Contact Mechanics*, Applied Mechanics Reviews **69**, 060804 (2017).
- [11] D. Tabor, *The hardness of metals*, Clarendon Press, Oxford, UK (1951).
- [12] B. Lorenz, B.N.J. Persson, *Leak rate of seals: Effective-medium theory and comparison with experiment*, The European Physical Journal E **31**, 159 (2010)
- [13] B. Lorenz, B.N.J. Persson, *Leak rate of seals: Comparison of theory with experiment*, Europhysics Letters **86**, 44006 (2009).
- [14] Martin H Müser, Wolf B Dapp, Romain Bugnicourt, Philippe Sainsot, Nicolas Lesaffre, Ton A Lubrecht, Bo NJ Persson, Kathryn Harris, Alexander Bennett, Kyle Schulze, Sean Rohde, Peter Ifju, W Gregory Sawyer, Thomas Angelini, Hossein Ashtari Esfahani, Mahmoud Kadkhodaei, Saleh Akbarzadeh, Jiunn-Jong Wu, Georg Vorlauffer, Andras Vernes, Soheil Solhjoo, Antonis I Vakis, Robert L Jackson, Yang Xu, Jeffrey Streater, Amir Rostami, Daniele Dini, Simon Medina, Giuseppe Carbone, Francesco Bottiglione, Luciano Afferrante, Joseph Monti, Lars Pastewka, Mark O Robbins, James A Greenwood, *Meeting the contact-mechanics challenge*, Tribology Letters **65**, 118 (2017).
- [15] BNJ Persson Theory of rubber friction and contact mechanics, The Journal of Chemical Physics **115**, 3840 (2001)
- [16] A. Almqvist, C. Campan, N. Prodanov and B.N.J. Persson, *Interfacial separation between elastic solids with randomly rough surfaces: Comparison between theory and numerical techniques*, Journal of the Mechanics and Physics of Solids **59**, 2355 (2011).
- [17] B.N.J. Persson, *Leakage of metallic seals: role of plastic deformations*, Tribology Letters **63**, 42 (2016).
- [18] F. Pérez Ràfols, R. Larsson, S. Lundström, P. Wall, A. Almqvist, *A stochastic two-scale model for pressure-driven flow between rough surfaces*, Proceedings of the Royal Society A: Mathematical, Physical and Engineering Sciences, 472(2190), 20160069 (2016).
- [19] A. Almqvist, F. Sahlin, R. Larsson, S. Glavatskih, *On the dry elasto-plastic contact of nominally flat surfaces*, Tribology international, 40(4), 574-579 (2007).
- [20] A.R. Hinkle, W.G. Nöhring, R. Leute, T. Junge, L. Pastewka, *The emergence of small-scale self-affine surface roughness from deformation*, Science advances **6**, 0847 (2020).
- [21] S.P. Venugopalan, N. Irani, L. Nicola, *Plastic contact of self-affine surfaces: Persson's theory versus discrete dislocation plasticity*, Journal of the Mechanics and Physics of Solids **132**, 103676 (2019).
- [22] N. Irani, L. Nicola, *Modelling surface roughening during plastic deformation of metal crystals under contact shear loading*, Mechanics of Materials **132**, 66 (2019).
- [23] S.P. Venugopalan, L. Nicola, *Indentation of a plastically deforming metal crystal with a self-affine rigid surface: A dislocation dynamics study*, Acta Materialia **165**, 709 (2019).
- [24] P.R. Nayak, *Random Process Model of Rough Surfaces*, J. Lubrication Technol. **93**, 398 (1971).
- [25] G. Carbone, B. Lorenz, B.N.J. Persson, A. Wohlers *Contact mechanics and rubber friction for randomly rough surfaces with anisotropic statistical properties*, The European Physical Journal E **29**, 275 (2009).
- [26] B.N.J. Persson, O. Albohr, U. Tartaglino, A.I. Volokitin and E. Tosatti, *On the nature of surface roughness with application to contact mechanics, sealing, rubber friction and adhesion*, J. Phys.: Condens. Matter **17**, R1 (2005)

- [27] A. Tiwari, A. Wang, M.H. Müser, B.N.J. Persson, *Contact Mechanics for Solids with Randomly Rough Surfaces and Plasticity* Lubricants **7**, 90 (2019).
- [28] E. Broitman, *Indentation Hardness Measurements at Macro-, Micro-, and Nanoscale: A Critical Overview* Tribol Lett **65**, 23 (2017).
- [29] F. Sahlin, R. Larsson, A. Almqvist, P. M. Lugt, P. Marklund, *A mixed lubrication model incorporating measured surface topography. Part 1: theory of flow factors*, Proceedings of the Institution of Mechanical Engineers, Part J: Journal of Engineering Tribology, 224(4), 335-351 (2010).
- [30] S. P. Venugopalan, M. H. Müser, L. Nicola, *Green's function molecular dynamics meets discrete dislocation plasticity*, Modelling and Simulation in Materials Science and Engineering, 25(6), 065018 (2017).
- [31] B. Weber, T. Suhina, T. Junge, L. Pastewka, A. M. Brouwer, D. Bonn, *Molecular probes reveal deviations from Amonton's law in multi-asperity frictional contacts*, Nature communications 9(1), 1-7 (2018).
- [32] V. A. Babeshko, O. V. Evdokimova, O. M. Babeshko, *On a mechanical approach to the prediction of earthquakes during horizontal motion of lithospheric plates*, Acta Mechanica, 229(11), 4727-4739 (2018).
- [33] D. Ernens, F. Pérez Ràfols, D. Van Hoecke, R. F. Roijmans, E. J. van Riet, J. B. Vande Voorde, M. Vanderschueren, *On the Sealability of Metal-to-Metal Seals With Application to Premium Casing and Tubing Connections*, SPE Drilling & Completion (2019).
- [34] A. Ghanbarzadeh, A. Hassanpour, A. Neville, *A numerical model for calculation of the restitution coefficient of elastic-perfectly plastic and adhesive bodies with rough surfaces*, Powder technology, 345, 203-212 (2019).
- [35] F.J. Fischer et. al., IFAS, Aachen University, Germany.